Femtosecond pump-probe spectroscopy and time-resolved photoluminescence of an $In_xGa_{1-x}N/GaN$ double heterostructure

C. K. Choi, B. D. Little, Y. H. Kwon, J. B. Lam, and J. J. Song
Center for Laser and Photonics Research and Department of Physics, Oklahoma State University, Stillwater, Oklahoma 74078-0444

Y. C. Chang
Department of Physics and Materials Research Laboratory, University of Illinois at Urbana-Champaign, Urbana, Illinois 61801-3080

S. Keller, U. K. Mishra, and S. P. DenBaars
Electrical and Computer Engineering and Materials Department, University of California, Santa Barbara, California 93106
(Received 4 October 2000; revised manuscript received 2 January 2001; published 5 April 2001)

We report a study of the carrier dynamics in an $In_{0.18}Ga_{0.82}N$ thin film photoexcited well above the band gap using nondegenerate pump-probe spectroscopy and time-resolved photoluminescence (TRPL) for carrier densities ranging from 10^{17} to 10^{19} cm^{-3} at 10 K. At carrier densities greater than 4×10^{18} cm^{-3}, optical gain occurs across the entire band tail region after ~2.5 ps time delay, when the hot carriers completely fill these states. From TRPL measurements performed in the surface emission geometry, we observed stimulated emission (SE) with a ~28 ps decay time. Since this SE has a threshold density of 1×10^{18} cm^{-3}, which is larger than the total density of localized states, and the SE spectra at early time delays are quite different from the spontaneous emission spectra, we attribute the SE to the recombination of an electron-hole plasma from renormalized band-to-band transitions.

DOI: 10.1103/PhysRevB.63.195302 PACS number(s): 78.47.+p, 72.20.Jv, 71.35.Lk, 71.35.Ee

The desire for ever higher resolution printing, read-write laser sources for high-density information storage on magnetic and optical media, and sources for secure intersatellite communications has fueled an interest in semiconductor lasers operating at shorter wavelengths. A long-lived continuous-wave blue $In_xGa_{1-x}N$ quantum well (QW) diode laser grown on a sapphire substrate was recently demonstrated at room temperature.[1] Despite extensive studies on the optical properties of $In_xGa_{1-x}N$ ternary alloys as the active light-emitting medium, the optical gain and stimulated emission (SE) mechanisms in these technologically promising new sources are still unclear. A major issue related to carrier dynamics is the many-body Coulomb interaction among electrically injected or photogenerated carriers in localized and extended states, given the high-carrier densities (larger than 10^{19} cm^{-3}) (Ref. 1) required to achieve lasing in present devices.

In this paper, we report a study of the carrier dynamics in an $In_xGa_{1-x}N$ thin film for carrier densities varying from 10^{17} to 10^{19} cm^{-3} photoexcited well above the band edge, using femtosecond nondegenerate pump-probe (PP) spectroscopy and time-resolved photoluminescence (TRPL) measurements at 10 K. Through these measurements, we explored not only the early-stage thermalization processes of the hot carriers, but also the spectral and temporal properties of the recombination processes, both as functions of carrier density.

The sample used in this paper is a nominally undoped 0.1 μm-thick $In_{0.18}Ga_{0.82}N$ layer grown by metalorganic chemical vapor deposition at 800 °C. The structure consists of a 20 nm GaN buffer layer grown on *c*-plane sapphire followed by a 1.8 μm GaN layer, a 50 nm GaN:Si (Si $\sim10^{18}$ cm^{-3}) layer, the 0.1 μm $In_{0.18}Ga_{0.82}N$ active layer, and a 50 nm GaN:Si (Si$\sim10^{19}$ cm^{-3}) cap layer. The average In composition was measured using high-resolution x-ray diffraction, assuming Vegard's law. We note that the actual InN fraction could be smaller due to systematic overestimation when using Vegard's law for this strained material system.[2] Since the $In_{0.18}Ga_{0.82}N$ conduction-band edge lies at a lower energy than the GaN:Si donor states, electrons from the donors will move into the $In_{0.18}Ga_{0.82}N$ region. The self-consistent potential seen by an electron in the double heterostructure can be modeled by an effective-mass theory that takes into account the exchange-correlation potential within the local-density approximation. We use the same numerical method described in Ref. 3 for modeling heavily doped semiconductor multiple-quantum wells (MQW's). At low temperature (T$\approx$10 K), most of the carriers remain trapped at the GaN:Si donor sites with only a small fraction migrating into the $In_xGa_{1-x}N$ layer. The amount of charge transfer is determined by requiring the Fermi level to be the same across the GaN and $In_xGa_{1-x}N$ layers (about 30 meV below the GaN conduction-band minimum that is taken to be zero in this calculation). The resulting self-consistent potential (solid curve) and carrier density (dashed curve) are shown in Fig. 1. For the heavily doped GaN cap layer, donor electrons within 2.2 nm from the front $GaN/In_xGa_{1-x}N$ interface are depleted, contributing to the two-dimensional (2D) carrier density of 1.1×10^{12} cm^{-2} in the left triangular $In_xGa_{1-x}N$ QW. For the less heavily doped GaN layer under the $In_xGa_{1-x}N$ layer, donor electrons within 15 nm from the back $In_xGa_{1-x}N/GaN$ interface are depleted, contributing to the 2D carrier density of 7.5×10^{11} cm^{-2} in the right triangular $In_xGa_{1-x}N$ QW. The total 2D carrier density in the $In_xGa_{1-x}N$ layer is 1.85×10^{12} cm^{-2}, which is not enough to substantially screen the Coulomb interaction among photo-excited carriers.

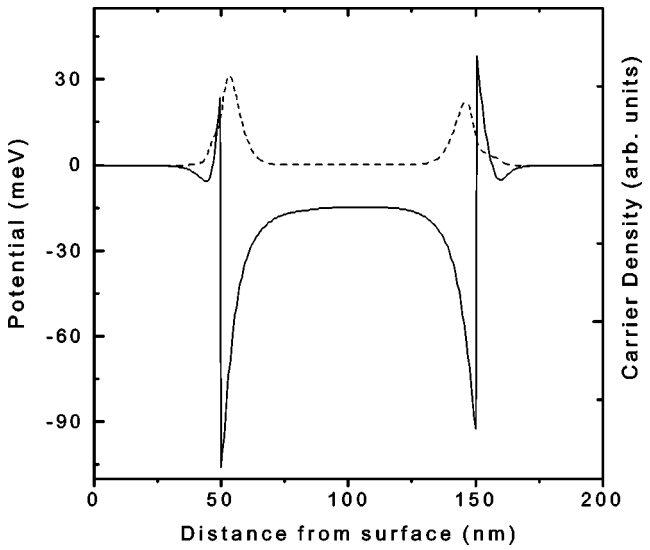

FIG. 1. Self-consistent potential profile seen by an electron across the $In_xGa_{1-x}N$ layer (solid line). Also shown is the carrier distribution (dashed line).

Femtosecond PP spectroscopy measurements were carried out with a 1 kHz regenerative amplifier (REGEN) used to create pulses with a full width at half maximum (FWHM) of 100 fs at a wavelength of 800 nm. These pulses were fed into an optical parametric amplifier to create pulses with a FWHM of 355 fs (measured by difference-frequency mixing in a BBO crystal) at 3.345 eV (295 meV above the absorption edge of the excited $In_xGa_{1-x}N$ sample at 10 K) with a bandwidth of 25 meV. This beam was used as the pump source to excite carriers above the $In_{0.18}Ga_{0.82}N$ band gap. The leftover output from the REGEN was frequency doubled to 400 nm and then used to create a broadband continuum probe source with a FWHM of 350 fs. The pump and probe beams were orthogonally polarized, and the angle between them was 15°. Neutral density filters were used to attenuate the probe beam so that it would not alter the optical properties of the sample. The probe beam was focused to a 150 μm diameter spot on the sample, and the transmitted light was collected and focused into a spectrometer with an attached charge-coupled device detector. A pump spot size of 300 μm was chosen to minimize the variations in pump beam intensity and to average out the effect of In compositional fluctuations across the probed region. The optical delay between the pump and probe was controlled using a computerized step motor. TRPL measurements were also performed in the surface emission geometry using a streak camera with a monochromator. The pump spot size was 150 μm in diameter and the overall time resolution for TRPL measurements was about 60 ps. For consistency, the same excitation energy was used for PP and TRPL experiments.

Differential transmission spectra (DTS) (Ref. 4) measure the difference between the probe transmission with and without the pump:

$$\mathrm{DTS} = \Delta T/T_0 = \left[\exp\left\{ -\int_0^d dz\, \Delta\alpha(z) \right\} \right] - 1. \qquad (1)$$

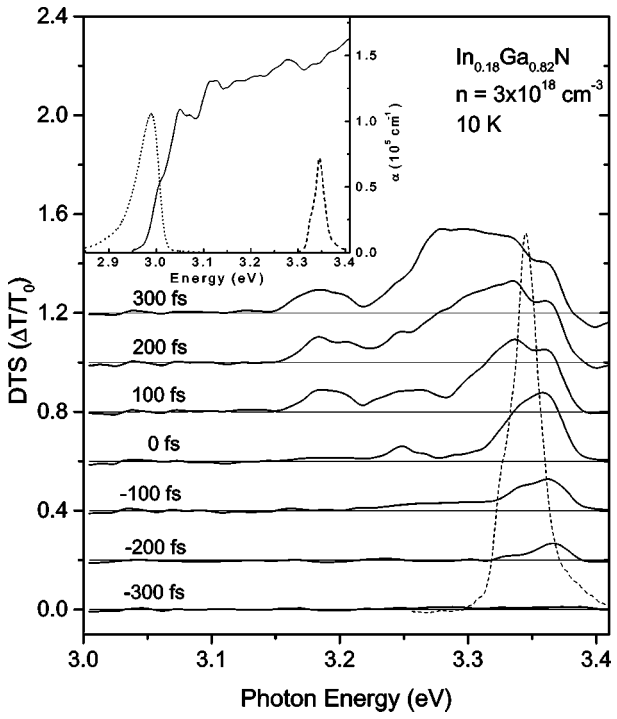

FIG. 2. Differential transmission spectra (pump-induced transmission change $\Delta T/T_0$) of a 0.1 μm $In_{0.18}Ga_{0.82}N$ active layer at 10 K for an average carrier density of 3×10^{18} cm^{-3} showing the ultrafast near-zero-delay dynamics. The dashed line shows the pump spectrum. The DTS curves are displaced vertically for clarity. The inset shows the absorption (solid line), PL (dotted line), and pump spectra for the pump-probe spectroscopy (dashed line).

where T, T_0, $\Delta\alpha(z)$, and d are the transmitted probe intensity with and without the pump, the pump-induced absorption change at depth z (measured from the front side interface), and the sample thickness, respectively. For an active layer thickness of 0.1 μm with an absorption coefficient of 1.5×10^5 cm^{-1} at the excitation energy, our sample is optically thick, so the photogenerated carrier density depends on the depth z, which leads to a depth-dependent absorption coefficient $\alpha(z)$. Figure 2 shows the DTS at early time delays for an average carrier density of 3×10^{18} cm^{-3} in the active layer, as estimated from band filling.[5] Using this average carrier density and assuming an exponential decrease in the photogenerated carrier density with depth, we estimate the carrier density at the front side interface ($z=0$ nm) and at the back-side interface ($z=100$ nm) to be 5.7×10^{18} cm^{-3} and 1.3×10^{18} cm^{-3}, respectively. We see in the inset that the low-density photoluminescence (PL) peak (dotted line) is significantly Stokes shifted ($\sim$58 meV) with respect to the fundamental absorption edge. This behavior arises from the combined effects of the large band bending near the interfaces and In compositional fluctuations[6–9] in this mixed semiconductor alloy. We take zero time delay to be at the approximate maximum of the pump pulse. For time delays of less than -200 fs, no significant band-filling effects were observed.

The DTS at -200 fs shows a spectral hole burning[10] that is initially peaked at the high-energy tail of the pump pulse.

At -100 fs, a broad low-energy tail arises from the fast interaction of photoexcited carriers with the previously existing electrons, illustrated in Fig. 1. We clearly observed two successive LO-phonon emission processes via the Fröhlich interaction at 0 and 100 fs time delays. At 0 fs, a broad peak at 3.25 eV arises from the emission of single LO-phonons, and at 100 fs, another broad peak occurs at 3.18 eV because of two successive LO-phonon emissions. The spacing is approximately equal to the expected $In_{0.18}Ga_{0.82}N$ LO-phonon energy of 89 meV, which is estimated by a linear interpolation of the values of 92 (Ref. 11) and 74 meV (Ref. 12) for GaN and InN, respectively. However, the successive LO-phonon emission does not necessarily mean that relaxation processes of the hot carriers can be explained by a simple LO-phonon cascade model. Considering the nonthermal carrier distribution on this time scale of less than 200 fs, and the decrease in the joint density of states with decreasing photon energy (which causes the DTS values to increase), only a small fraction of the hot carriers should be involved in the successive LO-phonon emissions. Similarly observed LO-phonon replicas during the pump duration was previously reported in GaAs at a carrier density of 8×10^{14} cm^{-3}.[13]

As shown in Fig. 2, the cooling processes of most of the carriers begin after the initial buildup of carriers by the pump. Carrier-carrier interactions that cause the gradual broadening of the nonthermal carrier distribution and electron-phonon scattering by both the Fröhlich and the deformation-potential mechanisms provide the most relevant relaxation processes. Compared to the rapid hot carrier redistribution in GaAs (Ref. 14) over a wide energy range within 100 fs at a lower excitation density, Fig. 2 shows that the hot carriers relax very slowly toward the band edge. This is mainly caused by the hot phonon effect,[15] since the electrons lose energy to LO-phonons very slowly when the LO-phonons are as hot as the electrons. Previously, a slow hot carrier relaxation in this material due to the hot phonon effect has been reported at 300 K.[16]

The carrier dynamics near the absorption edge of the sample is shown in Fig. 3 as a function of time delay for average carrier densities of (a) 4×10^{18} cm^{-3} and (b) 4×10^{17} cm^{-3}. The arrows indicate the effective mobility edge[17] (E_{em}) of the sample, which was determined by the excitation energy dependence of the PL peak position as detailed in Ref. 18. For an average carrier density of 4×10^{18} cm^{-3}, the average interparticle distance of about 3 nm is approximately equal to the exciton Bohr radius in GaN. Thus, the hot carriers of Fig. 3(a) form an electron-hole plasma (EHP), while a coexistence of correlated states (excitons) and uncorrelated electron-hole pairs is possible at the average carrier density of Fig. 3(b). As the hot carriers relax toward the band edge, the band gap reduces, leading to induced absorption near and below the absorption edge appearing after ~1.3 ps, as shown in Figs. 3(a) and 3(b). Subsequently, the induced absorption reduces and turns into optical gain (or induced transparency) due to band filling by the hot carriers. The weak modulation in the resulting gain spectra comes from the Fabry-Perot modes of the sample structure. As shown in Fig. 3(a), optical gain across the entire band tail is evident at an average carrier density of 4×10^{18} cm^{-3}, and has a maximum value of $\sim1.2\times10^{4}$ cm^{-1} at 2.5 ps. Previous studies of PP spectroscopy on bulk GaAs (Ref. 19), $GaAs/Al_xGa_{1-x}As$ MQW's (Ref. 20), and $In_xGa_{1-x}N/GaN$ MQW's (Ref. 21) also showed optical gain near the band edge. Assuming that a single round-trip condition in the sample growth direction is satisfied and that there is no loss due to absorption in the $In_xGa_{1-x}N$ active layer, a threshold gain for vertical-cavity SE was found to be 10^5 cm^{-1} for 20% reflectivity at both side interfaces and a gain length (active layer thickness) of 0.1 μm.[22] Since this threshold gain value is one order of magnitude larger than the experimentally observed optical value of $\sim1.2\times10^4$ cm^{-1} at an average carrier density of 4×10^{18} cm^{-3}, it may not be possible to achieve vertical-cavity SE from optical pumping except under extremely high-excitation densities. At 3 ps in Fig. 3(b), there are still available states below E_{em}, but most of the carriers are situated at energies above 3.04 eV. This means that the total density of localized states due to In compositional fluctuation is less than 4×10^{17} cm^{-3}. To be consistent, the TRPL mea-

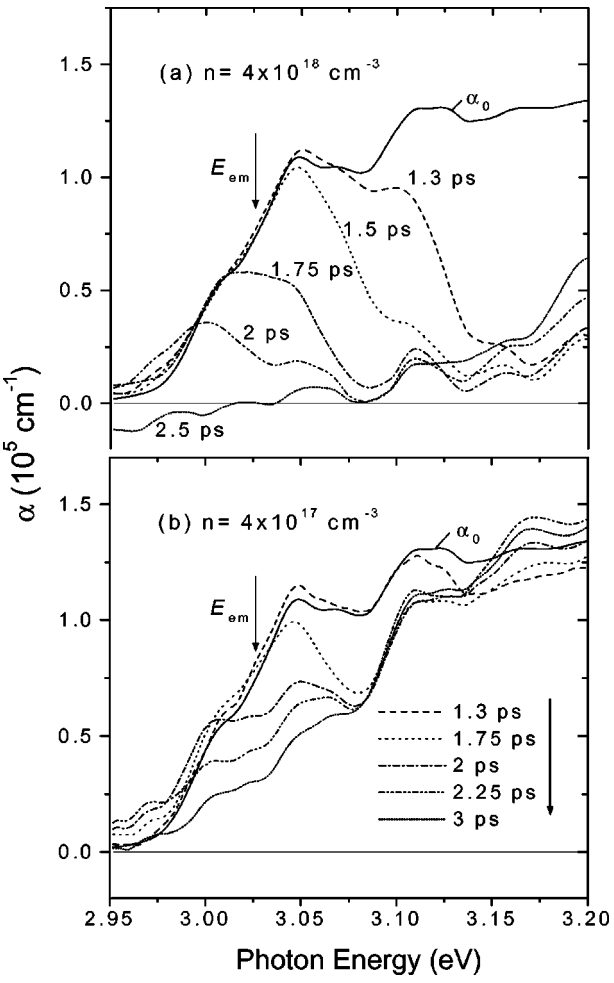

FIG. 3. Absorption spectra near the fundamental absorption edge of an $In_{0.18}Ga_{0.82}N$ active layer as a function of time delay for average carrier densities of (a) 4×10^{18} cm^{-3} and (b) 4×10^{17} cm^{-3}. The solid lines represent the values taken without the pump (α_0). The arrows indicate the effective mobility edge (see text).

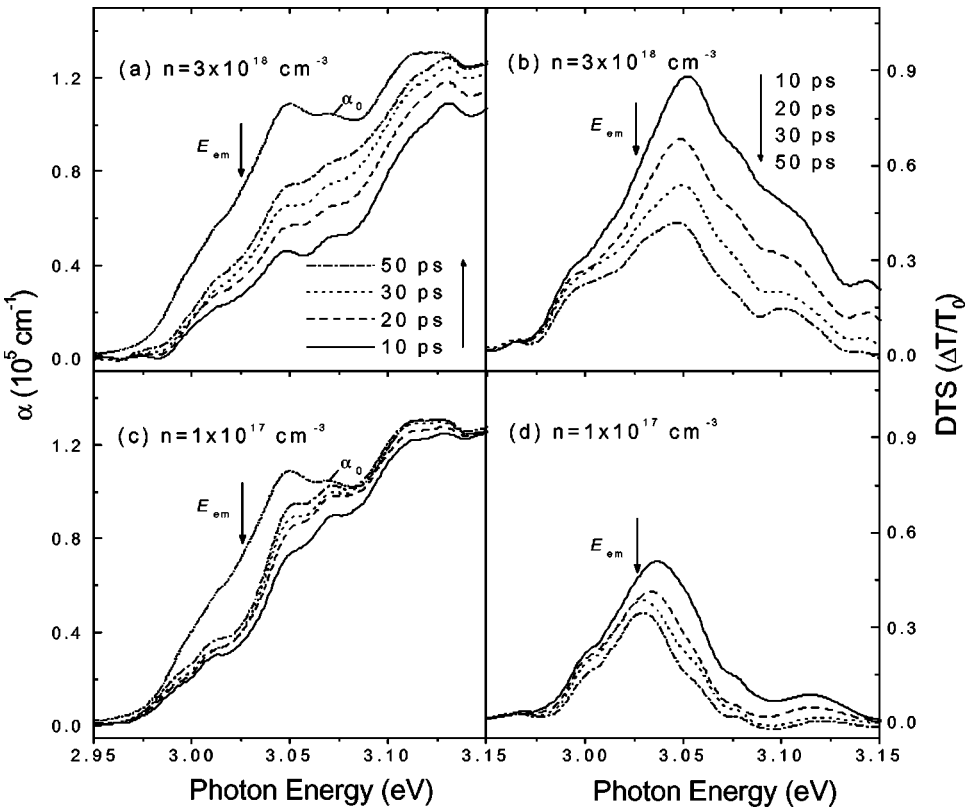

FIG. 4. Absorption spectra and their corresponding differential transmission spectra near the band tail region of an $In_{0.18}Ga_{0.82}N$ active layer as a function of time delay for average carrier densities of (a, b) 3×10^{18} cm^{-3} and (c, d) 1×10^{17} cm^{-3}. The arrows indicate the effective mobility edge.

surements seen below show that the PL peak position does not shift up to an average carrier density of 1×10^{17} cm^{-3}, but it has a significant blueshift at an average carrier density of 5×10^{17} cm^{-3} due to band filling of the localized states. Therefore, we estimate the total density of localized states in this sample to be between 1×10^{17} cm^{-3} and 4×10^{17} cm^{-3}.

The energy relaxation rate of hot carriers depends strongly on the number of available lower-energy states and decreases quickly with decreasing energy within the band tail due to the reduced density of the final states. Absorption spectra and their corresponding DTS near the band tail region at time delays from 10 to 50 ps are shown in Fig. 4. The recovery from bleaching effects at an average carrier density of 1×10^{17} cm^{-3} is much slower than at 3×10^{18} cm^{-3} [note the bleaching across the entire tail region at 2.5 ps in Fig. 3(a)]. This indicates that a very fast and efficient carrier depopulation process, i.e., SE, exists at an average carrier density of 3×10^{18} cm^{-3}. At average carrier densities greater than 1×10^{18} cm^{-3}, our TRPL measurement results show that most of the carriers disappear through SE with a $\sim$28 ps decay time (see below). On the other hand, it takes about 1.8 ps for the hot carriers to relax to the absorption edge, as shown in Fig. 3. Compared to this time scale, the relaxation processes shown in Fig. 4 are very slow. In fact, we see in Fig. 4(d) a clamping of carrier relaxation near $E_{\rm em}$ at an average carrier density of 1×10^{17} cm^{-3}, though the localized states below $E_{\rm em}$ are able to accommodate most electron-hole pairs produced at this density. This may be evidence for an analogous mobility edge in the Mott-Anderson picture of localization[23] in view of hot carrier relaxation.

Figure 5 shows (a) the carrier density dependence of the time-integrated PL spectra and (b) their corresponding temporal responses. The effective PL lifetimes (τ_0 and τ_1) as determined by single (for average carrier densities 2×10^{16}, 1×10^{17}, and 5×10^{17} cm^{-3}) and double (for 2×10^{18} and 1×10^{19} cm^{-3}) exponential fittings are indicated in Fig. 5(b). We observed SE above an average carrier density of 1×10^{18} cm^{-3}. Above the SE threshold density, the integrated PL intensity exhibits a superlinear growth as the carrier density increases. Compared to other III-V semiconductors, the observed SE threshold density is rather large, but this can be easily attributed to the large effective masses in this system, which make it difficult to reach population inversion.[24] According to Ref. 25, the filling of localized band-edge states is a prerequisite for achieving lasing in $In_xGa_{1-x}N$ QW laser diodes. Because the SE lifetimes are less than our system resolution of $\sim$60 ps, we obtained the decay constants using a deconvolution technique.

Spontaneous emission can be attributed to the well-known phenomenon of recombination of localized carriers (or excitons) in random potential wells induced by In compositional fluctuations,[6–9] since the strain-induced piezoelectric effect[26] in an 80-nm-thick layer of $In_xGa_{1-x}N$ is much smaller than in an $In_xGa_{1-x}N$/GaN MQW.[27] With the laser tuned to the absorption edge of 3.05 eV shown in Fig. 3, we performed time-integrated four-wave mixing on this sample at low-excitation densities. We found that the signal at 10 K is not sensitive to detuning, which results from In compositional fluctuation, and it has a polarization dephasing time of 150 fs assuming a homogeneous broadening similar to GaN.[28] This indicates that the absorption enhancement near the band edge is due to the excitonic ground state. The dephasing time of

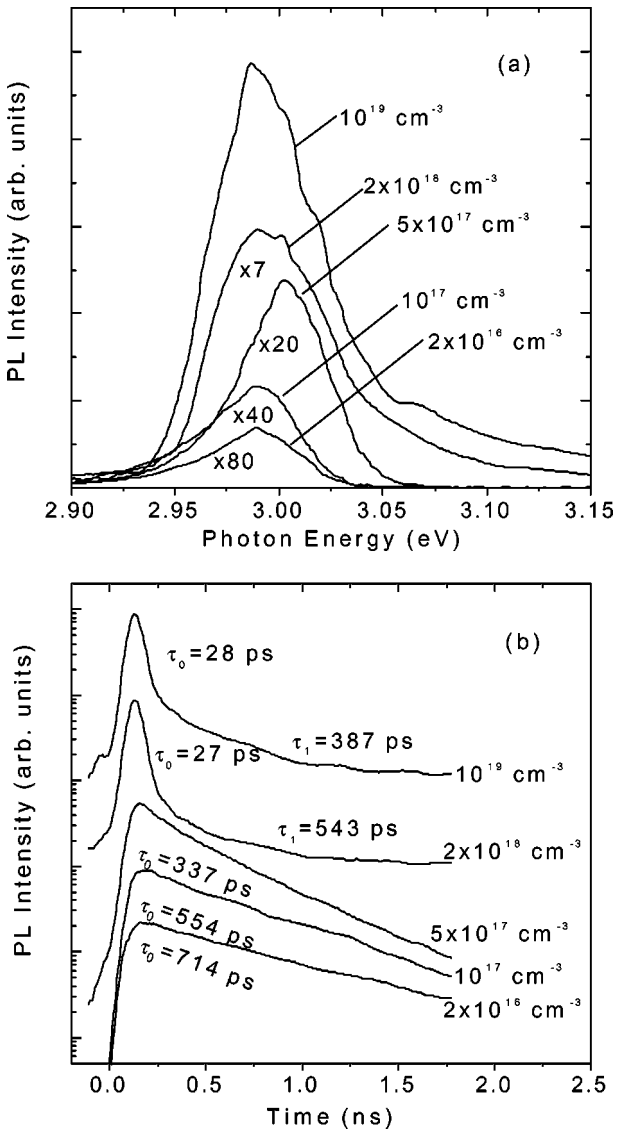

FIG. 5. (a) Time-integrated PL spectra and (b) their time-resolved PL intensities at various carrier densities. The PL spectra at different carrier densities in Fig. 5(a) have been rescaled as indicated. The average threshold carrier density for stimulated emission was found to be 1×10^{18} cm^{-3}.

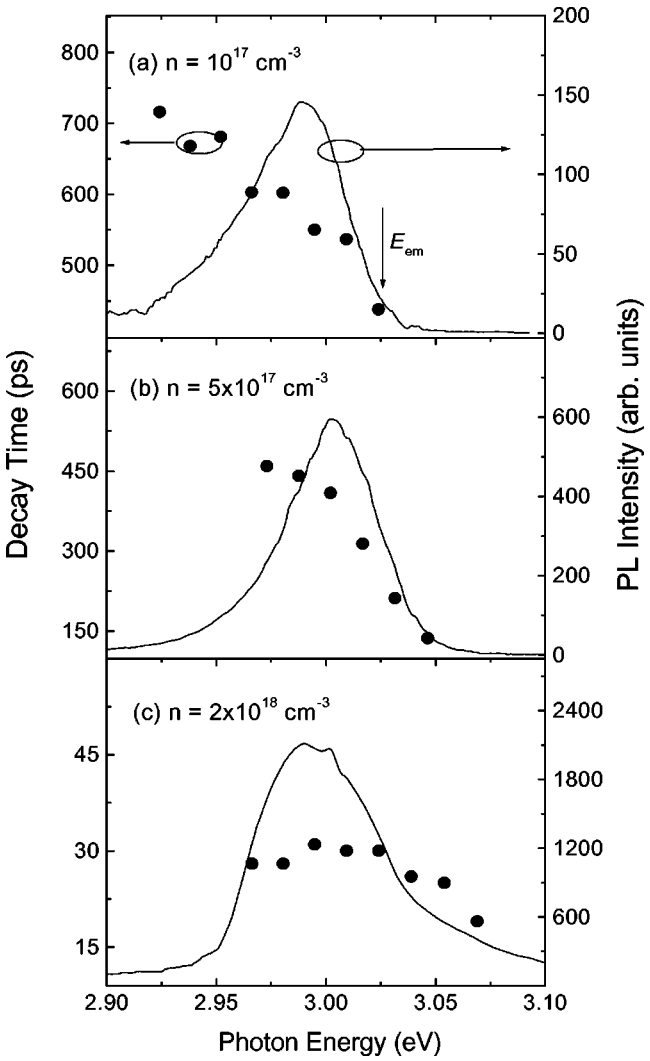

FIG. 6. The effective recombination lifetime (determined by curve fitting to exponential decay) as a function of emission energy for average carrier densities of (a) 1×10^{17}, (b) 5×10^{17}, and (c) 2×10^{18} cm^{-3}. The solid lines are the corresponding time-integrated PL spectra. The arrow indicates the effective mobility edge.

excitonic continuum states is expected to be much smaller. For instance, the dephasing time in pure GaAs was found to be less than 11 fs.[29] Therefore, piezoelectric fields should play only a minor role in this 0.1 μm-thick $In_xGa_{1-x}N$ material system. According to a simple model,[17] the density of states in the band tail quickly decreases with increasing activation energy, resulting in a lower density of final states for acoustic phonon-assisted relaxation or tunneling.[30,31] Thus, the average spatial separation between sites with deeper potential wells increases.[32] This causes a smaller tunneling probability per available site, and hence, a longer effective PL lifetime at lower energy. For carriers with energies above E_{em}, the decay is most likely dominated by the rapid nonradiative transfer to lower-localized states. As a result, the time-resolved spectrum shifts toward lower energy with increasing time delay, as shown in Figs. 6(a) and 6(b).

The temporal PL traces for carrier densities above the SE threshold density show in Fig. 5(b) two distinct decay constants: a short component for fast SE and a long component for subsequent spontaneous emission. Consistent with the occurrence of optical gain over a wide spectral region and the fast recovery from bleaching effects above the SE threshold density seen in PP spectroscopy, SE occurs from 2.95 eV to well above the absorption edge with decay constants of 27–28 ps, as shown in Fig. 6(c). Figure 7 shows the detailed temporal evolution of both the (a) SE and (b) spontaneous emission. The top curve on each graph is taken at the peak of the TRPL decay curve. The maximum PL intensity in the TRPL decay curve at an average carrier density of 1×10^{19} cm^{-3} occurs about 28 ps faster than at an average carrier density of 5×10^{17} cm^{-3}. Considering our system resolution, the actual temporal evolution of the SE can be faster than the time delays in Fig. 7(a). If the spontaneous emission and SE originate from the same mechanism, they

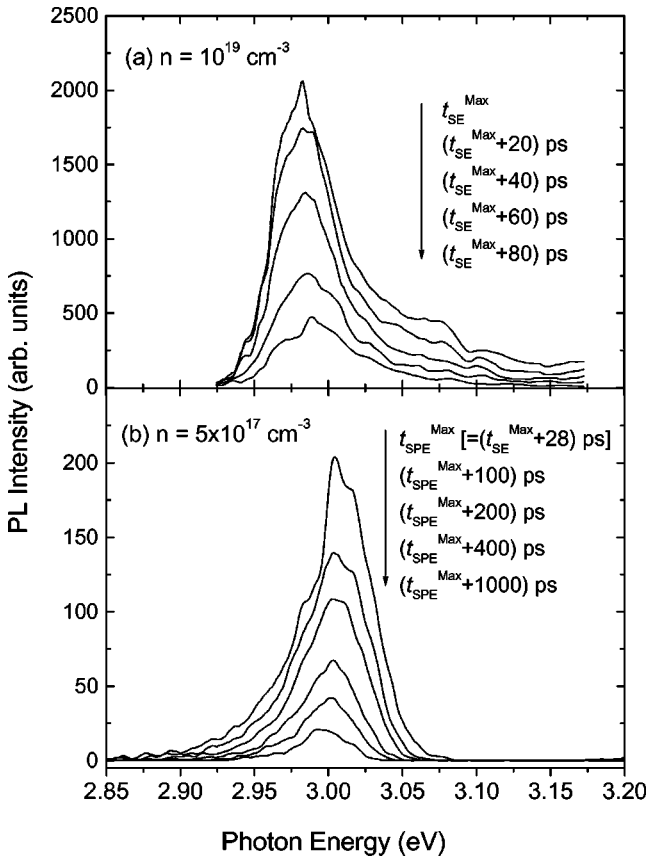

FIG. 7. Temporal evolution of (a) stimulated emission at an average carrier density of 1×10^{19} cm^{-3} and (b) spontaneous emission at an average carrier density of 5×10^{17} cm^{-3}. The top curve on each graph is taken at the peak of the time-resolved PL decay curve.

should have similar spectral shapes. However, the SE spectra at early time delays and the spontaneous emission spectra shown in Fig. 7 are quite different, indicating that the SE does not result from recombination of carriers in localized states. The temporal behavior of the SE peak shown in Fig. 7(a) can be well understood in terms of an EHP recombination from renormalized band-to-band transitions, where one expects such a blueshift as the number of carriers decreases through the SE with increasing time delay. This is consistent with our previous conclusion that the total density of localized states is less than 4×10^{17} cm^{-3}, and thus, SE must be dominated by carriers in extended states at these high densities.

We note that a previous study of SE as a function of excitation length for an $In_xGa_{1-x}N$/GaN MQW by nanosecond pulse excitation in the side pumping geometry was performed in Ref. 9, where the SE was shown to result from the recombination of carriers in localized states. Reference 9 also shows that the SE threshold density quickly decreases and the peak position redshifts with increasing excitation length (from 500 to 2500 μm) due to reabsorption in the photoexcited region. Since the experimentally observed optical gain value of $\sim10^4$ cm^{-1} shown in Fig. 3(a) is not enough to allow SE in the sample growth direction, we consider the SE observed in this study to be in-plane traveling light, which is scattered vertically by unintentionally formed crystal imperfections. The degree of localization in $In_xGa_{1-x}N$ active layers depends very much on the mean In molar fraction and the growth conditions. For the same $In_xGa_{1-x}N$/GaN double heterostructure (DH) used in this study and an $In_xGa_{1-x}N$/GaN MQW sample that has the same InN fraction and similar Si doping concentration in the barriers, Ref. 9 shows that the band-tail states are significantly larger in the $In_xGa_{1-x}N$/GaN MQW than in the $In_xGa_{1-x}N$/GaN DH. This is most likely due to the increased number of interfaces in the MQW compared to the DH, which leads to larger potential fluctuations. Therefore, both a small total density of localized states and a high SE threshold density resulted from a small optical gain length due to the crystal imperfections contribute to the fact that an EHP recombination from the renormalized band-to-band transition is responsible for SE in the $In_xGa_{1-x}N$/GaN DH discussed in this paper.

In conclusion, we studied the hot carrier dynamics in an $In_xGa_{1-x}N$ thin film photoexcited well above the band edge at 10 K under high-carrier densities. At a carrier density of 3×10^{18} cm^{-3}, we clearly observed two successive LO-phonon emission processes via the Fröhlich interaction at 0 and 100 fs time delays. As the hot carriers relax, optical gain across the entire band tail and even above the absorption edge occurs at 2.5 ps time delay. This gain results in stimulated emission that has a $\sim$28 ps decay time constant and a threshold density of 1×10^{18} cm^{-3}, which is larger than the total density of localized states induced by In compositional fluctuations. We attribute the stimulated emission to the recombination of an electron-hole plasma from renormalized band-to-band transitions.

This work was supported by BMDO, AFOSR, ONR, and NSF.

[1] S. Nakamura, MRS Internet J. Nitride Semicond. Res. **2**, 5 (1997).

[2] W. R. L. Lambrecht, Solid-State Electron. **41**, 195 (1997); T. Takeuchi, H. Takeuchi, S. Sota, H. Sakai, H. Amano, and I. Akasaki, Jpn. J. Appl. Phys., Part 2 **36**, L177 (1997); C. Wetzel, T. Takeuchi, S. Yamaguchi, H. Katoh, H. Amano, and I. Akasaki, Appl. Phys. Lett. **73**, 1994 (1998).

[3] Y. C. Chang and H. Yao, Phys. Rev. B **54**, 11 517 (1996).

[4] J. Shah, *Ultrafast Spectroscopy of Semiconductors and Semiconductor Nanostructures* (Springer-Verlag, Berlin, 1996), p. 23.

[5] Because of a large uncertainty in the quantum efficiency of the electron-hole pair generation and experimental difficulties in measuring the reflectance and transmittance of the sample, we calculated the carrier density using the band filling factor $[1-f_e-f_h]$ (see p. 22 in Ref. 3), assuming a simple parabolic band structure and equal occupation probabilities $[f_e=f_h]$ of electrons

and holes. In both PP and TRPL measurements, we measured nominal excitation energy densities. After a comparison between the calculated carrier density from the band filling factor and the measured nominal excitation energy density, we obtained a calibration factor. Then, carrier densities in TRPL measurements were determined with the calibration factor.

[6] S. Chichibu, T. Azuhata, T. Soda, and S. Nakamura, Appl. Phys. Lett. **69**, 4188 (1996).

[7] Y. Narukawa, Y. Kawahami, Sz. Fujita, Sg. Fujita, and S. Nakamura, Phys. Rev. B **55**, 1938 (1997).

[8] M. Smith, G. D Chen, J. Y. Lin, H. X. Jiang, M. A. Khan, and Q. Chen, Appl. Phys. Lett. **69**, 2837 (1996).

[9] Y. -H. Cho, T. J. Schmidt, S. Bidnyk, G. H. Gainer, J. J. Song, S. Keller, U. K. Mishra, and S. P. DenBaars, Phys. Rev. B **61**, 7571 (2000).

[10] J. L. Oudar, D. Hulin, A. Migus, A. Antonetti, and F. Alexandre, Phys. Rev. Lett. **55**, 2074 (1985).

[11] K. T. Tsen, D. K. Ferry, A. Botchkarev, B. Sverdlov, A. Salvador, and H. Morkoç, Appl. Phys. Lett. **72**, 2132 (1998).

[12] V. Yu. Davydov, V. V. Emtsev, I. N. Goncharuk, A. N. Smirnov, V. D. Petrikov, V. V. Mamutin, V. A. Vekshin, S. V. Ivanov, M. B. Smirnov, and T. Inushirma, Appl. Phys. Lett. **75**, 3297 (1999).

[13] C. Fürst, A. Leitenstorfer, A. Laubereau, and R. Zimmermann, Phys. Rev. Lett. **78**, 3733 (1997).

[14] T. Elsaesser, J. Shah, L. Rota, and P. Lugli, Phys. Rev. Lett. **66**, 1757 (1991).

[15] J. Shah, A. Pinczuk, A. C. Gossard, and W. Wiegmann, Phys. Rev. Lett. **54**, 2045 (1985).

[16] C. K. Sun, F. Vallée, S. Keller, J. E. Bowers, and S. P. DenBaars, Appl. Phys. Lett. **70**, 2004 (1997).

[17] E. Cohen and M. D. Sturge, Phys. Rev. B **25**, 3828 (1982); S. Permogorov and A. Reznitsky, J. Lumin. **52**, 201 (1992).

[18] A. Satake, Y. Masumoto, T. Miyajima, T. Asatsuma, F. Nakamura, and M. Ikeda, Phys. Rev. B **57**, 2041 (1998).

[19] T. Gong, P. M. Fauchet, J. F. Young, and P. J. Kelly, Phys. Rev. B **44**, 6542 (1991).

[20] C. V. Shank, R. L. Fork, R. Yen, J. Shah, B. I. Greene, A. C. Gossard, and C. Weisbuch, Solid State Commun. **47**, 981 (1983).

[21] Y. Kawakami, Y. Narukawa, K. Omae, S. Fujita, and S. Nakamura, Appl. Phys. Lett. **77**, 2151 (2000).

[22] D. M. Bagnall and K. P. O'Donnell, Appl. Phys. Lett. **68**, 3197 (1996).

[23] N. F. Mott and E. A. Davis, *Electronic Processes in Non-Crystalline Materials*, 2nd ed. (Oxford University, England, 1979).

[24] W. Fang and S. L. Chuang, Appl. Phys. Lett. **67**, 751 (1995).

[25] Y. -K. Song, M. Kuball, A. V. Nurmikko, G. E. Bulman, K. Doverspike, S. T. Sheppard, T. W. Weeks, and M. Leonard, Appl. Phys. Lett. **72**, 1418 (1998).

[26] T. Takeuchi, S. Sota, M. Katsuragawa, M. Komori, H. Takeuchi, H. Amano, and I. Akasaki, Jpn. J. Appl. Phys., Part 2 **36**, L382 (1997).

[27] E. Berkowicz, D. Gershoni, G. Bahir, E. Lakin, D. Shilo, E. Zolotoyabko, A. C. Abare, S. P. DenBaars, and L. A. Coldren, Phys. Rev. B **61**, 10 994 (2000).

[28] A. J. Fischer, W. Shan, G. H. Park, J. J. Song, D. S. Kim, D. S. Lee, R. Horning, and B. Goldberg, Phys. Rev. B **56**, 1077 (1997).

[29] P. C. Becker, H. L. Fragnito, C. H. Brito Crutz, R. F. Fork, J. E. Cunningham, J. E. Henry, and C. V. Shank, Phys. Rev. Lett. **61**, 1647 (1988).

[30] C. Gourdon and P. Lavallard, Phys. Status Solidi B **153**, 641 (1989).

[31] M. Oueslati, C. Benoit à la Guillaume, and M. Zouaghi, Phys. Rev. B **37**, 3037 (1988).

[32] J. A. Kash, A. Ron, and E. Cohen, Phys. Rev. B **28**, 6147 (1983).